

Flash Separation of Metals by Electrothermal Chlorination

Bing Deng^{1,2, #,*}, Shichen Xu^{1,#}, Lucas Eddy^{1,3}, Jaeho Shin¹, Yi Cheng¹, Carter Kittrell¹, Khalil JeBailey⁴, Justin Sharp¹, Long Qian¹, Shihui Chen¹, and James M. Tour^{1,4,5,6,*}

¹ Department of Chemistry, Rice University, Houston TX, 77005, USA.

² School of Environment, Tsinghua University, Beijing 10084, China.

³ Applied Physics Program, Rice University, Houston TX, 77005, USA.

⁴ Department of Materials Science and NanoEngineering, Rice University, Houston TX, 77005, USA.

⁵ Smalley-Curl Institute, Rice University, Houston TX, 77005, USA.

⁶ NanoCarbon Center and the Rice Advanced Materials Institute, Rice University, Houston TX, 77005, USA.

Those authors contributed equally: Bing Deng, Shichen Xu

* Corresponding authors: J.M.T. (tour@rice.edu), B.D. (dengbing@tsinghua.edu.cn)

Abstract Metal recycling plays a crucial role in mitigating the critical metals shortage and reducing reliance on primary mining. Current liquid hydrometallurgy involves significant water and chemical consumption with troublesome secondary waste streams, while pyrometallurgy lacks selectivity and requires substantial energy input. Here we develop an electrothermal chlorination and carbochlorination process, and a specialized compact reactor, for the selective separation of individual critical metals from electronic waste. Our approach uses programmable, pulsed current input to achieve precise control over a wide temperature range (from room temperature to 2400 °C), short reaction duration of seconds, and rapid heating/cooling rates (10^3 °C s⁻¹) during the process. The method capitalizes on the differences in the free energy formation of the metal chlorides. Once conversion to a specific metal chloride is achieved, that compound distills from the mixture in seconds. This allows for both thermodynamic and kinetic selectivity for desired metals with minimization of impurities.

Introduction

There is a pressing demand for metals in various electronic applications, superalloys, and renewable energy systems^{1,2}. Critical metals, aptly named from their significance in emerging technologies, are becoming harder to access and pose potential risks to the supply chain³. Within

the electronics industry, representative critical metals include indium (In), gallium (Ga), and tantalum (Ta), which find widespread applications in displays, semiconductors, lighting, and capacitors. For example, In, predominantly recovered from by-product residues during copper and zinc production⁴, is indispensable for producing indium-tin oxide (ITO) thin films, an essential component of transparent electrodes in displays and touch screens. Similarly, Ga, obtained as a by-product of commodity metal production⁵, is used in semiconductor forms such as gallium arsenide (GaAs), gallium nitride (GaN), and aluminum gallium indium phosphide (AlGaInP). Ta is extensively employed in capacitors for cellular phones and computers⁶, constituting 34% of total Ta consumption⁷. With the increasing demand for personal electronics, consumption of these critical metals is experiencing a sharp rise and previous supply chain dependability is ending⁸. Recovering critical metals from electronics at their end-of-life⁹, falls under the realm of urban mining¹⁰, thereby averting disruptions in the critical materials supply chains while mitigating the environmental impact of traditional mining and e-waste disposal¹¹.

Metals, in theory, are infinitely recyclable¹². However, current metal recycling and separation is inefficient due to the complexity of product design and restrictions on recycling technologies¹³. Conventional hydrometallurgical processes¹⁴, involving acid/alkaline leaching and liquid-liquid separation such as solvent extraction, exhibit good selectivity but are marked by significant water and chemical consumption, often leading to the generation of secondary wastewater streams¹⁵. Classical pyrometallurgical processes often lack selectivity, and the accumulation of alloying elements can result in the downgrading of metals¹⁶. Recently, a selective sulfidation was demonstrated to separate metals from a mixed metal oxide feedstock¹⁷.

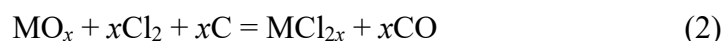
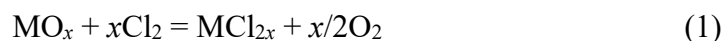
The chlorination process, commonly employed in extractive metallurgy for metal separations, has been industrially used to separate titanium (Ti) from its ores¹⁸. This process involves the reaction of various metals or metal compounds with chlorinating agents to form metal chlorides^{19,20}. Commercially, chlorination is conducted using fluidized bed²¹, typically operating within a temperature range of 900 to 1300 °C (ref²²). However, this limited temperature range restricts its wide applicability. Consequently, the chlorination process is practically employed in specific scenarios, such as for obtaining Ti and magnesium (Mg)¹⁹. In addition, chlorination at the lab scale is performed using indirect furnace heating. For example, In recovery from dental metal recycling sludges²³ and Ga recovery from solar cell waste materials²⁴ with ammonium chloride as the chlorinating agents has been described. The sluggish heating/cooling processes and long

treatment durations inherent in indirect heating reduce the energy efficiency and production rate of metal recovery, usually resulting in less economic incentives for use.

In addressing these limitations, we introduce direct electric heating^{25,26} or flash heating²⁷, characterized by ultrafast heating/cooling, rapid treatment, and widely tunable temperature, into the chlorination process. This integration is termed as electrothermal chlorination (ETC), and electrothermal carbochlorination (ETCC) when carbon is used as a reductant additive. These features enable us to overcome the constraints of the conventional chlorination process, significantly expanding its applicability in metals recovery and separation, increasing the production rate, and lowering the energy consumption. This is evidenced by the successful high-yield and high-purity recovery of In, Ga, and Ta from authentic e-wastes.

Thermodynamics and setup

In our initial phase, we undertook a thermodynamic analysis of the chlorination reactions of 34 metal oxides, using chlorine (Cl₂) as the chlorinating agent. This comprehensive study covered representative metals across *s*, *p*, and *d* blocks of the Periodic Table (Supplementary Note 1, Supplementary Data 1, Fig. 1a). Both the chlorination reaction (Eq. 1) and carbochlorination reaction (Eq. 2) were calculated:



These reactions fall into four groups based on their spontaneity under various temperature conditions: (1) The chlorination reaction is spontaneous at any temperature >0 °C; (2) The chlorination reaction is spontaneous with a lower limit temperature threshold (T_{crit}); (3) The chlorination reaction is spontaneous with an upper limit temperature threshold; (4) The chlorination reaction is not spontaneous under any readily accessible temperature but its carbochlorination reaction is spontaneous, where carbon serves as a reductant. This analysis reveals limitations in the conventional chlorination reaction. First, the temperature required for chlorination reactions can range from 400 to 2400 °C, thus many metal oxides cannot be chlorinated using a conventional furnace generally operating under 1500 °C. Secondly, the reaction temperature difference is narrow among some metal oxides, in which cases precise temperature control is required for the reactivity-based separation. Thirdly, for metals with similar chlorination reactivity trends, it is challenging to separate them solely based on thermodynamics.

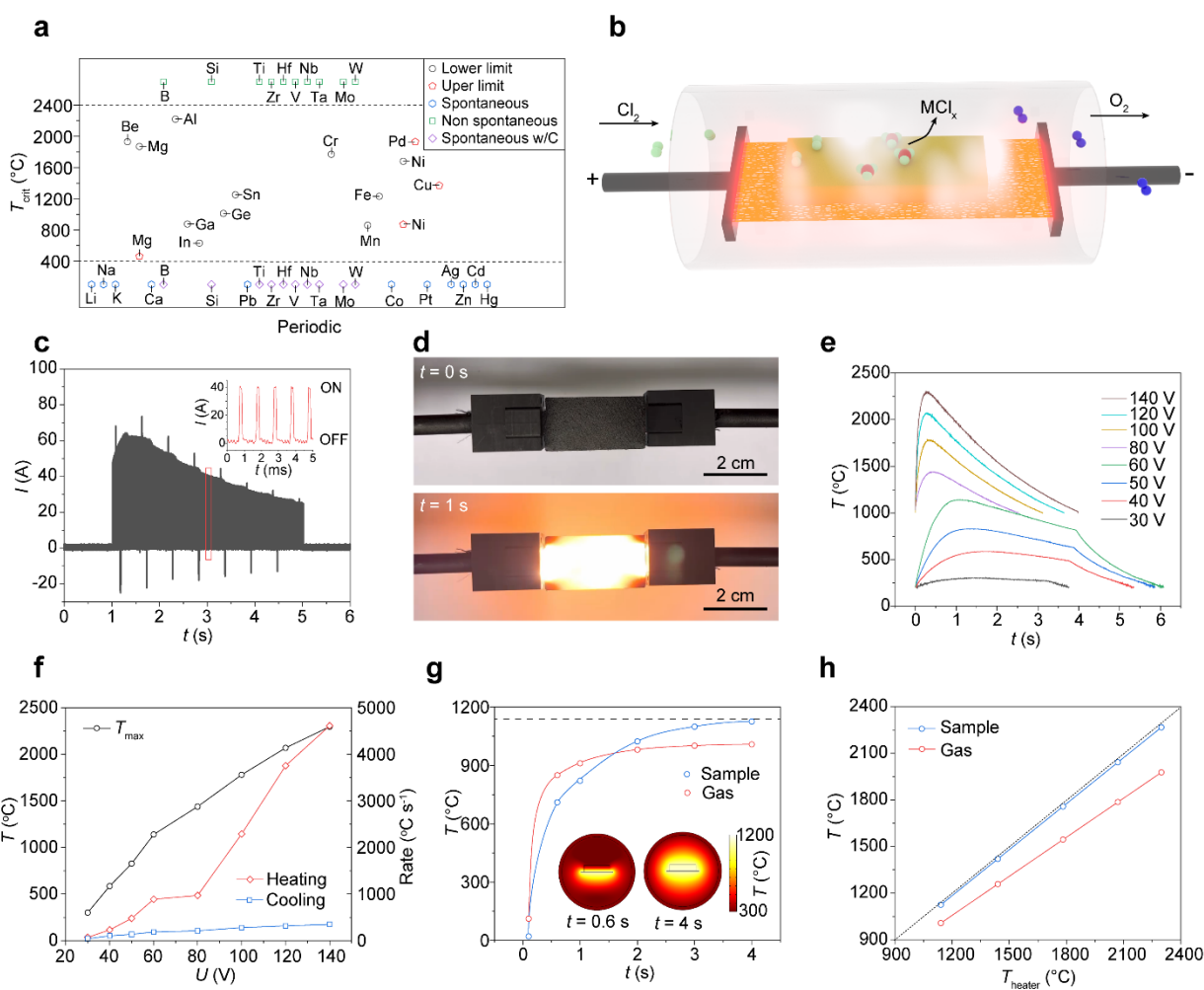


Fig. 1. Thermodynamics and setup of the ETC/ETCC process. (a) Critical reaction temperature (T_{crit}) of chlorination and carbochlorination for various metal oxides. The dashed lines denote the temperatures at 400 °C and 2400 °C. (b) Schematic of the ETC/ETCC process showing the metal chlorides vaporize and deposit on the surrounding quartz tube. (c) Current profile at 60 V, heater resistance of $\sim 1 \Omega$, and pulse duty cycle of 10%. Inset, the enlarged current profile in the red rectangle. (d) Pictures of the heater before (upper) and during (lower) electric heating. (e) Temperature profiles of the heater under different voltage inputs. (f) Maximum temperature (T_{max}) and heating/cooling rates of the heater under different voltage inputs. (g) Simulated temperature profiles of the sample and gas. The sample temperature is defined as its average temperature, and the gas temperature as the average of the gas within the diameter of carbon paper heater width, considering that only the gas close to the sample reacts. The dashed line denotes the heater temperature, which is fixed at 1141 °C, corresponding to the maximum temperature at 60 V input.

Inset, the simulated cross-sectional temperature distribution at $t = 0.6$ s and 4 s. **(h)** Correlation of sample and gas temperature versus the heater temperature (T_{heater}).

To overcome these obstacles, we introduced direct electric heating, proposing the ETC and ETCC processes (Fig. 1b, Supplementary Fig. 1). Diverging from conventional furnaces that use thermal convection, our method employs a carbon paper heater platform to heat the feedstock through thermal conduction. We built an electrical system (Supplementary Fig. 2) to deliver programmable current input to the heater (Fig. 1c), allowing ultrafast heating and cooling within seconds (Fig. 1d). The heater temperature can be precisely regulated through voltage input variation (Supplementary Fig. 3), enabling a wide temperature range from 400 to 2500 °C (Figs. 1e-f). The maximum temperature is mainly controlled by the voltage input. ETC/ETCC presents several superior features, addressing conventional furnace heating limitations. First, the high temperature capability up to 2500 °C (Fig. 1f) permits chlorination for almost all metal oxides (Fig. 1a). For example, using the ETC process, we show that the Cr_2O_3 can be converted to CrCl_3 at a temperature of >1770 °C (Supplementary Fig. 4), which is beyond the temperature range of typical furnace heating. Secondly, precise temperature control by just tuning the voltage input (Fig. 1f) facilitates the separation of metals with a narrow reaction window. Thirdly, the precise temperature control would also contribute to metal separation based upon vapor pressure difference of chlorides (Supplementary Fig. 5). Lastly, ultrafast heating (up to ~ 4500 °C s^{-1}) and cooling (~ 500 °C s^{-1}) rates (Fig. 1f) permit kinetic selectivity, allowing reactions with similar thermodynamics profiles to be distinguished based upon their rates and activation energy differences.

In the ETC/ETCC configuration, metal oxide precursors (mixed with carbon for ETCC) and Cl_2 gas underwent heating by the carbon paper heater. We conducted simulations to elucidate the details of the sample and surrounding Cl_2 gas heating process dynamics (Supplementary Note 2, Supplementary Tables 1-2, Supplementary Fig. 6). The carbon paper transfers heat to the solid sample and the chlorine gas through conduction and convection, respectively. We fixed the heater temperature at $T_{\text{heater}} = 1141$ °C, which is the experimentally measured value under voltage input of $U = 60$ V (Fig. 1f). The sample and gas temperatures reach a plateau (~ 1141 °C) within ~ 4 s (Fig. 1g, Supplementary Fig. 7), in contrast to traditional indirect heating processes taking hours to achieve thermal balance, highlighting the rapid heating capability of the electrothermal process. This rapid heat transfer suggests the chlorination reaction is operating primarily under a

thermodynamic equilibrium. By varying the T_{heater} , the sample and gas temperatures closely follow the T_{heater} pattern (Fig. 1h, Supplementary Fig. 8), showcasing the precise reaction temperature controllability. Having established the thermodynamics, designed the equipment, and clarified heat transfer details, we transitioned to case studies focusing on recovery and separation of critical metals from authentic e-wastes.

In recovery from ITO-containing waste

In holds a crucial status as a technology-critical element, primarily employed in ITO, which therefore becomes the main waste for In recycling²⁸. ITO is composed of 90% In and 10% tin (Sn) in their oxide forms. We analyzed the thermodynamics of the chlorination reaction of In_2O_3 and SnO_2 using Cl_2 as the chlorinating agent (Fig. 2a). Within a temperature window of 630 to 1240 °C, In_2O_3 converts to InCl_3 , while SnO_2 remains unreacted. This allows the immediate evaporation of InCl_3 (b.p., 497 °C) as the volatile phase, facilitating the separation from SnO_2 (sublimes, 1800°C) based on their volatility difference. The corresponding voltage input range is between 90 and 110 V (Fig. 2b, Supplementary Fig. 9).

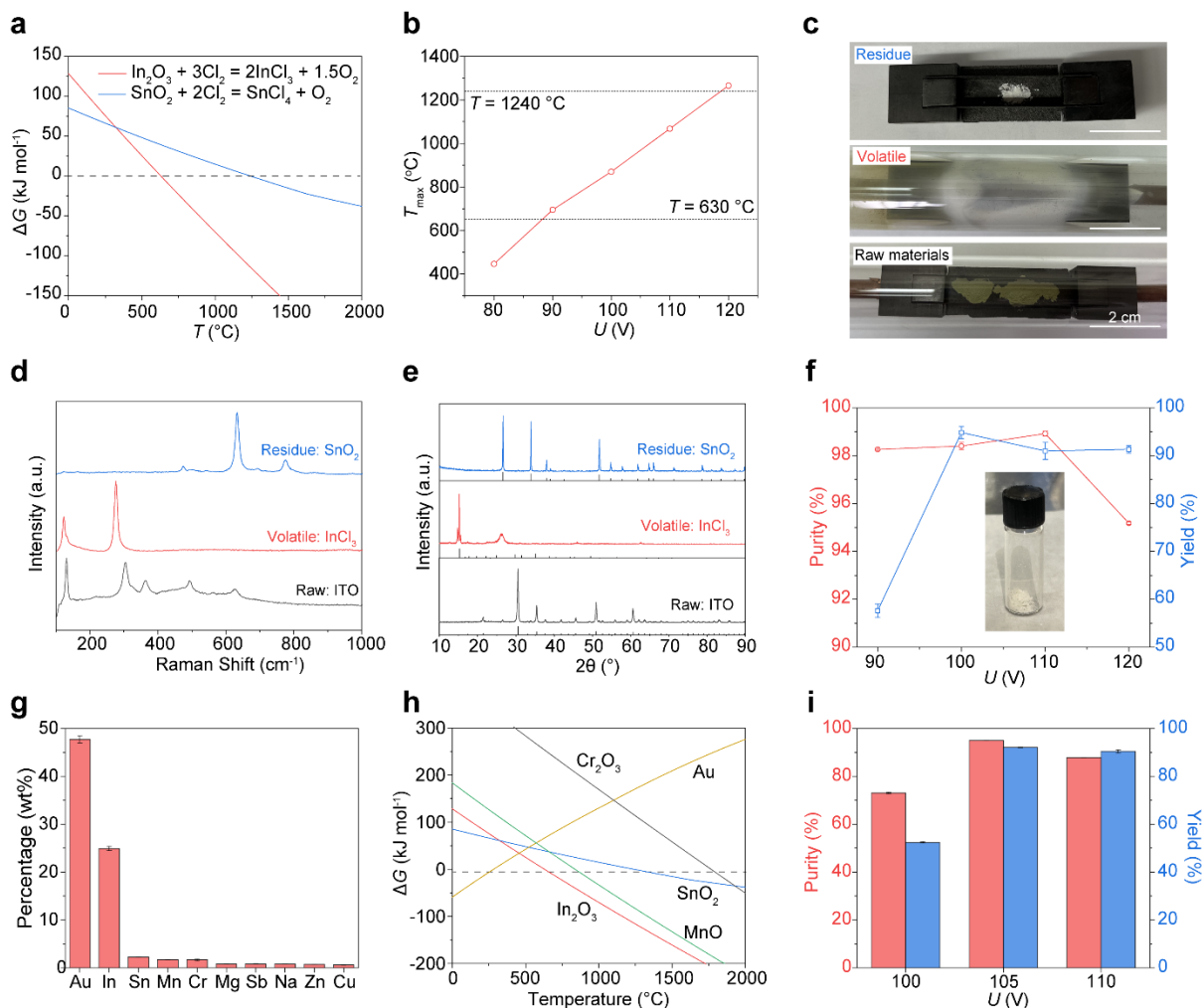


Fig. 2. Selective recovery of In from ITO-containing waste. (a) Calculated ΔG versus temperature for chlorination of In_2O_3 and SnO_2 . The dashed line denotes $\Delta G = 0$ kJ mol⁻¹. (b) Maximum temperature (T_{max}) of the carbon paper heater versus voltage input with the duty cycle of 5%. The bottom and top dash lines denote $T = 630$ °C and 1240 °C, respectively. (c) Picture of the ITO raw material (bottom), the volatile (middle), and the residue (top). (d) Raman spectra of the ITO raw material, InCl_3 volatile product, and SnO_2 residue. (e) XRD patterns of the ITO raw material (PDF#01-089-4597), InCl_3 volatile product (PDF#01-0170), and SnO_2 residue (PDF#00-021-1250). The broad peak at 26.3° is ascribed to Kapton tape used to seal the InCl_3 sample to slow its deliquescence. (f) Purity and yield of the product versus voltage input. Inset, the picture of InCl_3 obtained. (g) Major metal composition in the TCE waste. (h) ΔG of chlorination reaction versus temperature for main components in the TCE waste, including In_2O_3 , MnO , SnO_2 , Au, and

Cr₂O₃. The dash line denotes $\Delta G = 0 \text{ kJ mol}^{-1}$. (i) Recovery yield and purity of In from the TCE waste. The error bars in **f**, **g**, and **i** denote the standard deviation where $N = 3$.

To validate our approach, we controlled the voltage input at 100 V, demonstrating the feasibility of converting In₂O₃ to InCl₃ through the ETC process (Supplementary Fig. 10). Then, we used raw ITO as the precursor. After the ETC process, we obtained volatiles condensed on the quartz tube and residues remaining on the heater (Fig. 2c). Raman spectra and X-ray diffraction patterns (XRD) conclusively identified the volatiles as InCl₃ and the residue as SnO₂ (Figs. 2d-e). We further investigated the impact of voltage input on purity and yield (Fig. 2f). As voltage increases, the yield is improved due to the more complete reaction; however, excessive voltage input at 120 V leads to reduced purity because of the concurrent chlorination of SnO₂ (Fig. 2b). The optimized result exhibits 99% purity and 91% yield of In in the volatile product (Fig. 2f).

Transitioning to authentic e-waste, we focused on the recovery of In from used transparent conductive films (TCF). After removing plastic substrates by calcination (Supplementary Fig. 11), the resulting metal mixture primarily composed of Au, In, Sn, Mn, and Cr, among others. Total quantification through digestion followed by inductively coupled plasma mass spectrometry (ICP-MS) measurement indicated that In accounts for ~30 wt% among the metal content (Fig. 2g). We considered five primary metals with content >1 wt%, including Au, In, Sn, Mn, and Cr. Computational thermodynamic analysis of the chlorination reaction was conducted on Au, In₂O₃, SnO₂, MnO, and Cr₂O₃ (Fig. 2h). Within a temperature window of 630 to 830 °C, only In₂O₃ would be chlorinated and separated from other metals through evaporation (Supplementary Fig. 12). The effect of voltage input on In recycling performance was investigated (Fig. 2i, Supplementary Fig. 13). An insufficiently low voltage at 100 V led to inadequate temperature, chlorinating Au along with In₂O₃, resulting in low In product purity. Conversely, excessively high voltage input at 110 V caused the chlorination of SnO₂ and MnO, reducing the desired In product purity. At an optimal voltage of 105 V, we achieved the best overall performance, with 95% purity and 92% yield of In (Fig. 2i). The recovery yield can be further improved by adding carbon separators to retard the gas-phase loss of the desired product (Supplementary Fig. 14). This underscores the pivotal role of careful temperature control in the selective recovery of metals, a notable advantage of the ETC process.

Ga recovery from LED manufacturing wastes

The recovery of Ga from e-wastes offer an alternative solution to counterbalance the escalating demand for Ga in consumer electronics. We first used neat GaN to exemplify the feasibility of ETC (Supplementary Fig. 15). Then, we used LED manufacturing wastes as the resource for Ga recovery (Method, Supplementary Fig. 16). After removing the silicon substrate, we obtained a mixed metal powder predominantly composed of Ag, SiO₂, Au, and GaN, with Ga constituting ~30 wt% among the metal contents.

Thermodynamic analysis revealed that the chlorination of Ag and GaN is spontaneous over a wide range of temperatures, while SiO₂ and Au chlorination reaction is not spontaneous at temperatures >290 °C (Supplementary Fig. 17a). Despite the lack of thermodynamic differentiation between Ag and GaN chlorination, their chloride products, AgCl (b.p., 1550 °C) and GaCl₃ (b.p., 201 °C), exhibit significant differences in vapor pressure (Supplementary Fig. 17b), thereby ensuring their separation. ETC followed by selective evaporation from LED manufacturing wastes (Supplementary Fig. 17c), through an optimized voltage input, afforded Ga with 97.5% purity and 86.4% yield (Supplementary Figs. 17d-e). The near-absence of Ga in the residue confirmed the completeness of the reaction (Supplementary Fig. 18). Secondary wastewater streams and tailings are mitigated.

Ta recovery from waste capacitors

Ta is another technology-critical metal, primarily integral to electronic components as capacitors²⁹. The vast prevalence of Ta capacitors waste (TCW) in used small electrical appliances, with a high Ta content up to 45 wt%, positions them as a high-grade Ta resource³⁰. Prior to the ETC/ETCC recovery, the raw TCW were subjected to calcination in air to eliminate plastic and resin layers. This process yielded a finely powdered mixture, dominated by various metal oxides, including tantalum pentoxide (Ta₂O₅, Supplementary Fig. 19). Total quantification of metals in the powder discloses that Ta constitutes 37.8 wt% among metal contents, accompanied by other significant metal compositions (>1 wt%), including Si, Mn, Cu, Fe, and Ni (Fig. 3a).

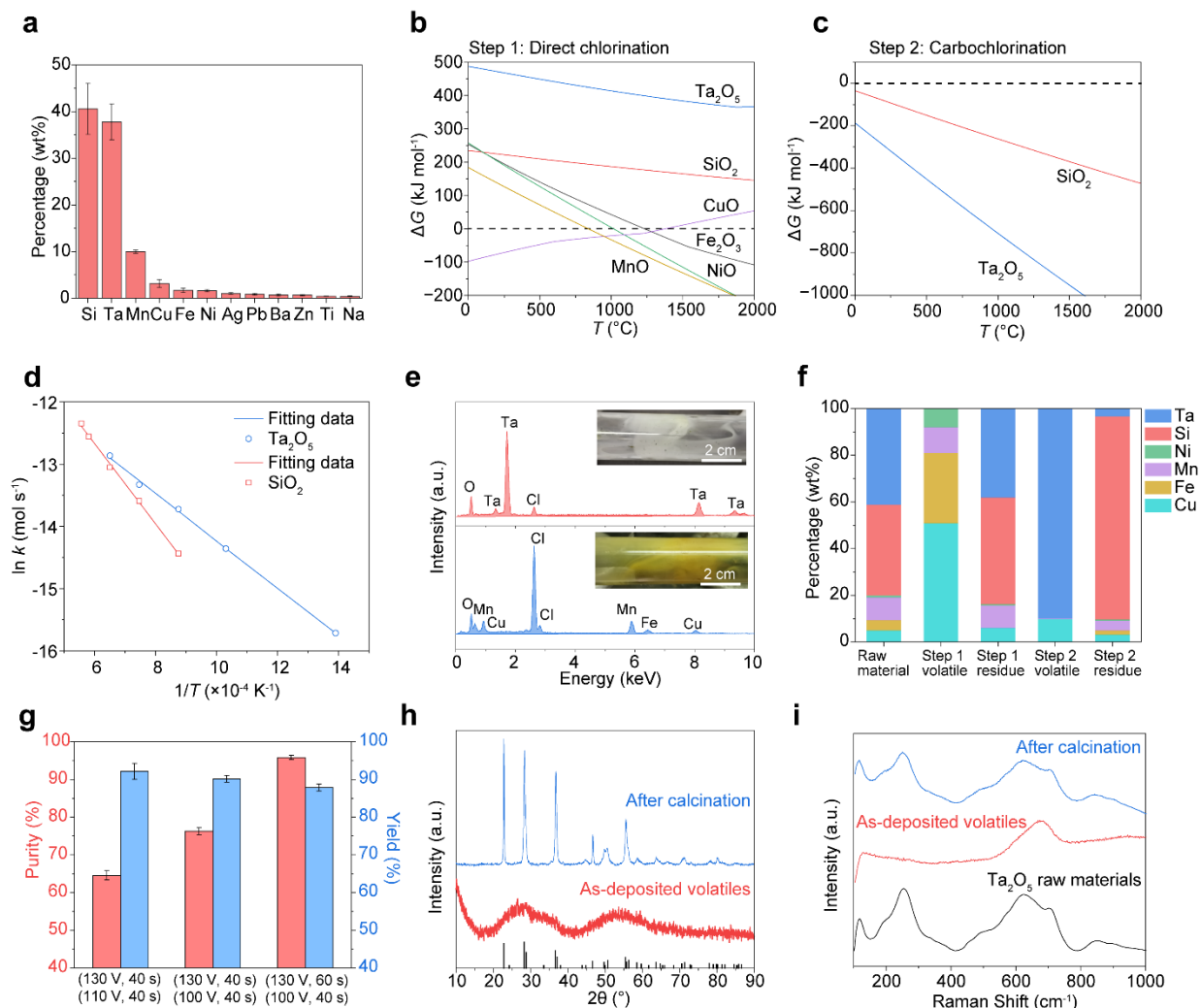


Fig. 3. Selective recovery of Ta from Ta capacitor waste. (a) Major metals present in the Ta capacitor waste. (b) ΔG of the chlorination reaction versus temperature for major metals in Ta capacitor waste, including Ta_2O_5 , SiO_2 , CuO , Fe_2O_3 , NiO , and MnO . The dashed line denotes $\Delta G = 0 \text{ kJ mol}^{-1}$. (c) ΔG of the carbochlorination reaction versus temperature for Ta_2O_5 and SiO_2 . The dash line denotes $\Delta G = 0 \text{ kJ mol}^{-1}$. (d) Kinetics of the carbochlorination of Ta_2O_5 and SiO_2 . The slopes of the fitted curves according to the Arrhenius equation where the activation energies are $\text{SiO}_2 = 53.6 \text{ kJ mol}^{-1}$ and $\text{Ta}_2\text{O}_5 = 31.6 \text{ kJ mol}^{-1}$. (e) EDS spectra of the first-step volatile (bottom) and the second-step volatile (top). Insets are the pictures of the volatiles condensed on the quartz tube; step 1 chlorination lower inset and step 2 carbochlorination upper inset. (f) Metal content percentages in Ta capacitor raw materials, step 1 chlorination volatile and residue, and step 2 carbochlorination volatile and residue. (g) Product purity and yield under different electrothermal chlorination conditions. The first row in the x-axis denotes the first step ETC parameters, and the

second row denotes the second step ETCC parameters. **(h)** XRD patterns of the as-deposited volatiles and that after calcination. The reference PDF of Ta₂O₅ is shown (01-082-9637). **(i)** Raman spectra of the Ta₂O₅ raw materials, as-deposited volatiles, and that after calcination. The error bars in **a** and **g** denote standard deviation where $N = 3$.

Computational thermodynamic analysis of the chlorination reactions for these metal oxides with Cl₂ delineated two groups (Fig. 3b): (1) CuO, Fe₂O₃, NiO, and MnO, with spontaneous chlorination reactions with specific temperature thresholds; and (2) Ta₂O₅ and SiO₂, with thermodynamically unfavorable chlorination reactions. Experimental verification through ETC of Ta₂O₅ with Cl₂ corroborated it as being unreactive (Supplementary Fig. 20). For Ta₂O₅ and SiO₂, the thermodynamics of their carbochlorination reactions were analyzed (Fig. 3c), revealing thermodynamic spontaneity for both oxides by ETCC. Despite the thermodynamic similarity, the substantial difference in Gibbs free energy change (ΔG) between SiO₂ and Ta₂O₅ suggests possible kinetic selectivity for their separation. To experimentally verify this, we mixed Ta₂O₅ with carbon (C) and conducted the ETCC reaction (Supplementary Fig. 21). Ta₂O₅ was successfully converted to a volatile product projected to be tantalum oxychlorides³¹, that can be collected through evaporation-condensation. SiO₂ underwent a similar treatment. Carbochlorination reaction kinetics were experimentally determined for SiO₂ and Ta₂O₅, from which we obtained the rate constants (Supplementary Note 3). Based on the Arrhenius equation, the activation energies (E_a) of carbochlorination reactions were calculated to be $E_a(\text{SiO}_2) = 53.6 \text{ kJ mol}^{-1}$ and $E_a(\text{Ta}_2\text{O}_5) = 31.6 \text{ kJ mol}^{-1}$ (Fig. 3d). The activation energy difference facilitates the kinetically controlled separation of Ta₂O₅ and SiO₂. To prove this, we mixed SiO₂ and Ta₂O₅ with C and conducted the ETCC reaction (Supplementary Fig. 22a). By precisely controlling the voltage at 100 V and corresponding temperature at $\sim 1050 \text{ }^\circ\text{C}$, Ta₂O₅ was selectively chlorinated and separated by evaporation from the unreacted SiO₂ residue (Supplementary Figs. 22b-c).

Leveraging the thermodynamic and kinetic selectivity, we devised a two-step strategy for Ta separation from TCW (Supplementary Fig. 23). In the first step, the ETC reaction at 1230 to 1380 $^\circ\text{C}$ converted CuO, Fe₂O₃, NiO, and MnO to their chlorides, which evaporated as the volatile phase. Ta₂O₅ and SiO₂ were unreactive and in the residue phase. Elemental dispersion spectroscopy (EDS, Fig 3e, bottom; Supplementary Fig. 24) and ICP-MS (Fig. 1f, step 1 volatile and residue) confirmed this enrichment and separation. In the second step, the ETCC reaction

involved mixing the first-step residue with C and then carbochlorination reaction. By controlling the electrothermal temperature at ~ 1050 °C, Ta_2O_5 was predominantly chlorinated and collected as the volatile phase (Fig. 3e, top; Fig. 3f, step 2 volatile), while SiO_2 remained predominantly in the residue (Fig. 3f, step 2 residue; Supplementary Fig. 25). After optimizing the voltage input and duration of the two-step strategy, we achieved the selective recovery of Ta from TCW with 96% purity and 88% yield (Fig. 3g). The obtained Ta product is an amorphous tantalum oxychloride, which easily converts into pure Ta_2O_5 through mild calcination in air (Figs. 3h-i).

Scale-up capability

The scalability of the ETC/ETCC process is critical for practical applications. Ensuring precise temperature control, a key factor in selective metal recovery, involves understanding the parameters influencing temperature. According to our theoretical analyses (Supplementary Note 4, The critical role of heater resistance in Joule heating), an optimal heater resistance exists for efficient energy conversion from electricity to heat. This value is determined by the electrical supply system, and the optimized resistance range of 0.5 to 2 Ω for the carbon paper heater platform. Consistency in heater resistance is vital during the scale-up process, which can be realized by maintaining the thickness and aspect ratio (defined as ratio of length to width, L/W) of the heater platform (Supplementary Note 4, Design of a carbon paper heater). In our initial experiments, we used a carbon paper heater with dimensions of 3×1 cm² (L/W), defined as scaling factor (S) of 1. To explore scalability, we used an enlarged heater while keeping the aspect ratio at 3. Under the same voltage input of 120 V, the larger-sized heater exhibited a lower temperature, a predictable outcome (Fig. 4a). A heat/temperature map varying with the size of the heater and the voltage input was constructed to guide the required voltage input during scale-up (Fig. 4b).

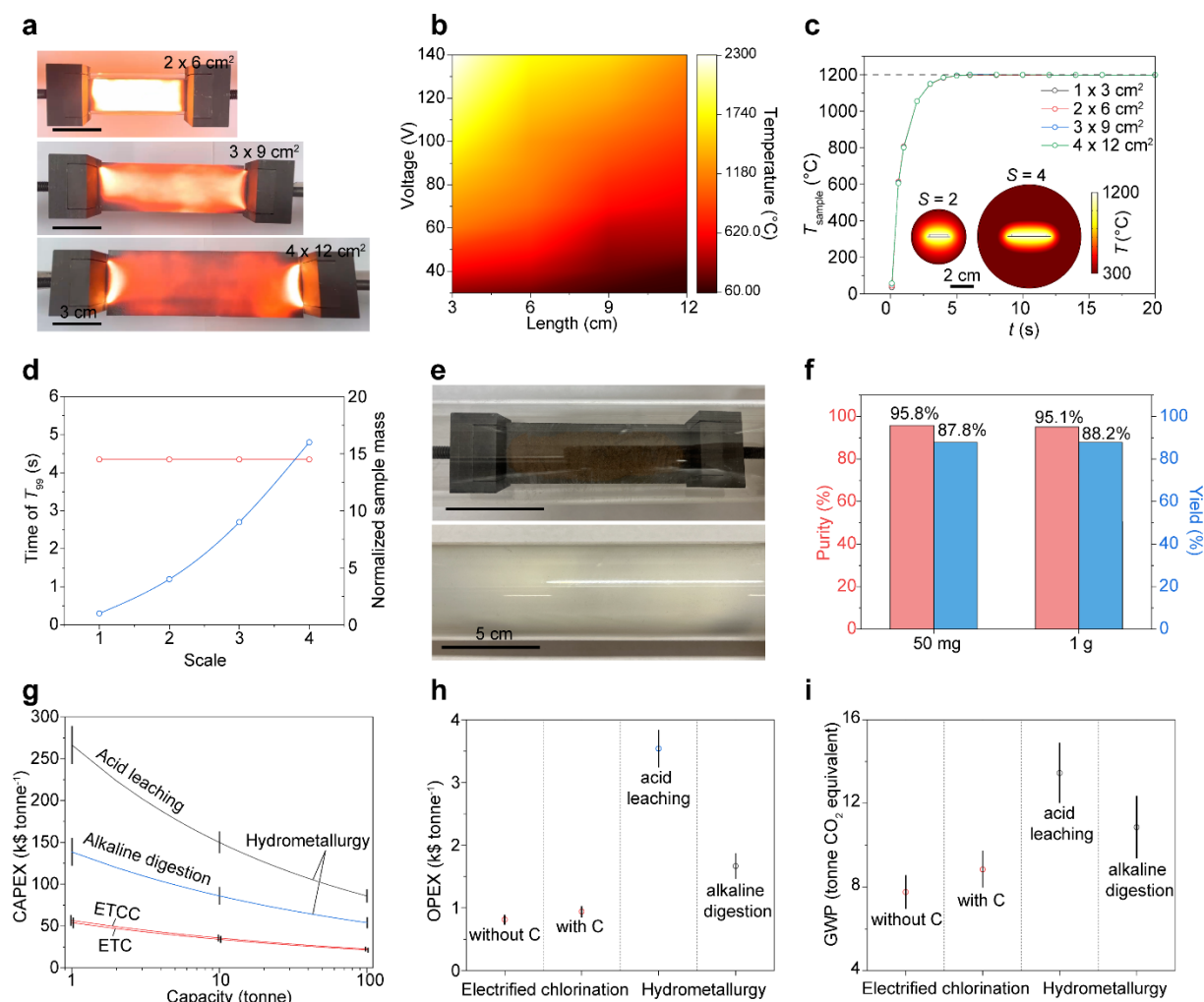


Fig. 4. Scalability, technoeconomic and sustainability considerations. (a) Pictures of carbon paper heaters under the same voltage input of 100 V, with sizes of $2 \times 6 \text{ cm}^2$, $3 \times 9 \text{ cm}^2$, and $4 \times 12 \text{ cm}^2$ ($W \times L$). (b) The heater temperature map versus voltage input and heater length. The thickness of the heater remains constant and its aspect ratio (L/W) is fixed to 3. (c) Simulated average temperature profile of sample with different heater scales (S). $S = 1$ means $1 \times 3 \text{ cm}^2$. The heater temperature is fixed to $1200 \text{ }^\circ\text{C}$. Inset, simulated temperature distribution for $S = 2$ and 4. (d) Time of T_{99} and the normalized sample mass varied with heater scale. The sample mass is defined as 1 at the scale of 1. (e) Picture of the raw TCW placed on the carbon heater with size of $3 \times 9 \text{ cm}^2$ (top) and the volatile deposited on the quartz tube after the second-step ETCC reaction (bottom). (f) Purity and yield of the Ta product recovered from the scaled-up batch at 1.0 g. (g) Capacity-dependent CAPEX of separation of binary metal oxides using the electrothermal chlorination (with and without carbon) and the hydrometallurgical processes (acid leaching and

alkaline digestion). **(h)** OPEX of separation of binary metal oxides using the electrothermal chlorination or the hydrometallurgical processes at capacity of 1 tonne. **(i)** GWP of separation of binary metal oxides using the electrothermal chlorination or the hydrometallurgical processes at capacity of 1 tonne. Error bars in **g**, **h**, and **i** denote one standard deviation, as determined through Monte Carlo uncertainty analysis.

After elucidating the size-dependent heater temperature, we analyzed the sample temperature through simulation (Supplementary Note 4, Simulation of the sample heating of upscaled sample). We first considered two-dimensional (2D) scale-up, where the sample length and width are proportionally enlarged according to the heater dimensions, while maintaining the sample thickness. The temperature profiles of the sample follow the same pattern across different scales (Fig. 4c, Supplementary Fig. 26). The metric, time of T_{99} , representing the time required to heat the sample temperature to 99% of the heater temperature, remained independent of scale despite the exponential increase in sample mass (Fig. 4d). This underscores the excellent scalability of electrical heating for chlorination. The three-dimensional (3D) scale-up, where all three dimensions of the sample are proportionally enlarged, was also analyzed. In this case, time of T_{99} is increased with the sample size (Supplementary Figs. 27-28). Nevertheless, the temperature reached a plateau within ~ 1 min for the upscaled sample, still outperforming indirect heating methods that take hours to reach thermal balance.

Last, to experimentally demonstrate scalability, the ETC/ETCC for selective metal recovery was increased to gram-scale, using a 2-inch (5.08 cm) tube reactor and a larger heater of $9 \times 3 \text{ cm}^2$ (L/W). The reactor was first used for ETC recovery of In from ITO at gram-scale (Supplementary Fig. 29a). Operating processes remained consistent with the small-scale reactions by using higher voltage inputs (Supplementary Table 3). Optimization resulted in a 98% purity and 91% yield of In (Supplementary Fig. 29b), comparable to small reactor results (Fig. 2f). A processing time of ~ 10 min equated to a productivity of 144 g per day from this laboratory reactor. Subsequently, we attempted to scale up the two-step ETC and ETCC process for selective recovery of Ta from TCW, also at gram-scale (Fig. 4e, Supplementary Fig. 30). We achieved 95.1% purity and 88.2% yield of Ta at the gram-scale, mirroring the results obtained at the 50 mg scale. This suggested the potential for further scaling the electrothermal reactor. The above analysis and

experiments validate the potential for scaling up the electrothermal reactor while mitigating secondary waste streams.

In our current experiments, we used chlorine gas as the chlorinating agent for the ETC/ETCC reaction. Unreacted chlorine can be easily recovered and recycled in an industrial implementation by condensation³² or adsorption/desorption cycle³³. While chlorine is often the preferred chlorinating agent on an industrial scale, other chlorinating agents like chloride or waste chlorine-containing plastics like polyvinyl chloride, can be used as the chlorinating agent¹⁰. Although we here demonstrated the selective recovery of one critical metal in e-waste, the ETC process is projected to be done in a continuous manner to selectively separate metals (Supplementary Fig. 31).

Technoeconomic consideration and environmental consideration

In evaluating the economic feasibility, we conducted a technoeconomic analysis (TEA) to compare the capital costs (CAPEX) and operating costs (OPEX) of the ETC/ETCC process with currently deployed hydrometallurgical processes (Supplementary Note 5). Two generic ETC and ETCC processes were considered, encompassing process blocks such as Cl₂ introduction, ETC or ETCC reaction, gas recovery, off-gas treatment, and post-treatment to obtain the metal oxide product (Supplementary Fig. 32, Supplementary Data 2). As counterparts, two hydrometallurgical processes, acid leaching followed by solvent extraction^{28,34} and alkaline digestion followed by selective leaching³⁵ (Supplementary Fig. 33, Supplementary Data 2), were comparatively analyzed. CAPEX was estimated using scaling factors ranging from 1 to 100 tonnes per year. Monte Carlo simulations were implemented for sensitivity analyses. The results indicated a reduction in CAPEX with increased capacity (Fig. 4g), showcasing the economy of scale. The ETC and ETCC processes were expected to exhibit a 20 to 40% reduction in CAPEX compared to hydrometallurgical processes (Fig. 4g, Supplementary Fig. 34). At a 1-tonne scale per year, the OPEX of the ETC and ETCC were ~\$800 and ~\$900, respectively (Fig. 4h, Supplementary Fig. 35). In contrast, the acid leaching and alkaline digestion processes exhibited OPEX of ~\$3500 and ~\$1700, respectively. The OPEX of the electrothermal process represented 23% to 56% of the hydrometallurgical processes. The economic benefit of the ETC/ETCC can be ascribed to the compact reactor design and reduced operating procedures. While we primarily used a capacitor system to provide direct current input for Joule heating, we showed that the alternating current is

also applicable (Supplementary Fig. 36). This can further reduce the equipment cost of the ETC/ETCC process.

A cradle-to-gate life-cycle assessment (LCA) was conducted, aiming to examine the environmental impacts and energy demands of the ETC/ETCC process (Supplementary Note 6, Supplementary Data 2). Acid leaching followed by solvent extraction, and alkaline digestion followed by selective leaching processes, served as representatives of hydrometallurgy for selective metal recovery. The functional unit was defined as the selective recovery of target metals from 1 tonne of mixed metal oxides. The global warming potential (GWP) of ETC and ETCC was estimated to be ~ 7.8 and ~ 8.8 tonnes, respectively, of CO₂ equivalent per tonne of feedstock (Fig. 4i, Supplementary Fig. 37), which are 19 to 42% lower than that of the acid leaching (~ 13.4 tonnes) and alkaline digestion (~ 10.9 tonnes). The cumulative energy demand (CED) for ETC/ETCC processes was $\sim 5 \times 10^4$ MJ per tonne of feedstock, reflecting a 26 to 65% reduction compared to hydrometallurgical processes (Supplementary Fig. 37). Notably, the ETC/ETCC process demonstrated significantly lower water resource depletion (WRD) compared to the conventional acid leaching process (Supplementary Fig. 37), owing to the minimal water consumption of the ETC/ETCC process. Considering that metal production constitutes a substantial part of global greenhouse gas (GHG) emission³⁶, the ETC/ETCC process holds promise as a sustainable metal separations method for a low-carbon-footprint metal industry.

Discussion

We compared the ETC/ETCC process with other indirect furnace heating-based chlorination processes for Ga, In, and Ta recovery from e-wastes^{20,23,24} (Supplementary Table 4). The ETC/ETCC process exhibits improvements regarding yield, purity, and production rate. If the three metals were mixed together, they can be successfully separated as well (Supplementary Fig. 38). Although we here primarily focused on the recovery of Ga, In, and Ta as critical metals in electronics, 12 metals in total were involved in this process, including In, Sn, Mn, Au, Ta, Si, Fe, Ni, Cu, Ga, Ag, and Cr. These metals serve as good representatives to demonstrate the generality of our approach: In, Sn, and Ga are *p*-block metals; Si is a metalloid; Mn, Ta, Fe, Ni, Cu, and Cr are transition metals; and Au, Ag are precious metals within the transition metal block.

The incorporation of direct electric heating into the chlorination process represents a transformative shift in metallurgy that could minimize supply chain shortage. The ability to

achieve ultrahigh temperature greatly expands the applicability of metal feedstocks; the precise temperature control enhances metal separations based on subtle differences in chlorination free energies of formation; the rapid heating and cooling rates permit kinetic selectivity, allowing chlorination reactions with similar thermodynamics to be distinguished based upon rate differences; and the high energy efficiency of electric heating makes the metal recovery process cost-effective. As a result, these performance improvements of ETC/ETCC processes greatly expand the generality, practicality and economic viability of chlorination metallurgy for metal recycling. While e-wastes were used in the current work, we envision that the process is applicable for industrial wastes such as coal fly ash³⁷ and bauxite residue³⁸, and even crude ores¹⁹, considering that metal oxides constitute the majority of those feedstocks.

Methods

Materials.

The chemicals used were In₂O₃ (MilliporeSigma, 99.998%), ITO (MilliporeSigma, -325 mesh, 99.99%), InCl₃ (MilliporeSigma, 98%), Ta₂O₅ (Sigma Aldrich, 99%), SiO₂ powder, and carbon black (Cabot, Black Pearls 2000). The carbon paper was purchased from FuelCellStore (Toray Carbon Paper 060). Carbon paper is chosen as the heater because it has appropriate resistance for Joule heating, it is highly graphitized material that is stable up to 3000 °C, and it is also chlorine-resistant (Supplementary Fig. 39). The TCF wastes for In recovery were purchased from eBay. The as-obtained TCF wastes were calcined at 800 °C in air for 2 h to remove the plastic substrate using a furnace (NEY 6-160A). The TCW for Ta recovery was purchased from eBay. The as-received TCW were calcined at 800 °C in air for 2 h to remove the plastic housings. The calcination step is required to remove the plastic so that the inorganic metal components are available for reaction with chlorine and to prevent extensive off-gassing during the electrothermal process. In practice, full-chain e-waste recycling involves an incineration step³⁹ to pyrolyze the organics and the thermal energy is recovered and used. Our process can follow analogously for the first step in the metal recovery. We here mimicked the LED manufacturing process to produce the wastes. Briefly, GaN (500 nm), Ag (500 nm), SiO₂ (500 nm), and Au (100 nm) layers were sequentially deposited on a pre-patterned silicon wafer. After lift-off, the mixed metal powders were collected and dried using an oven at 120 °C for 2 h. The as-obtained dry mixed metal powder was used for the Ga recovery (Supplementary Fig. 16a).

Chlorine supply system.

The scheme of the chlorine supply system is shown in Supplementary Fig. 1. A Cl₂ cylinder (MilliporeSigma, 99.5%, 85 psi, 454 g) was used to supply the Cl₂. Argon gas (Airgas, 99.99%) combined with the pumping system was used to purge the system, which is essential to remove moisture and air before introducing Cl₂. The vacuum pump is made of stainless steel, and an ascarite halogen trap was affixed at the inlet of the pump to absorb most of the unreacted Cl₂. A reservoir is used between the Cl₂ cylinder and the gas pipelines, to provide limit Cl₂ release in case of cell failure. The CGA-180 fitting with PTFE O-ring was used to connect the Cl₂ cylinder and the reservoir. The tubing and fitting of the chlorine supply system are made of stainless steel. The regulators and pressure gauges are made of Monel or stainless steel that are designed for corrosive gases. A needle valve combined with the rotameter was used to control the Cl₂ gas flow rate. A sodium hydroxide (NaOH) bath was used to absorb the unreacted Cl₂ gas. We noted that when industrialized, the unreacted Cl₂ can be easily recovered and reused.

Electrical system.

The diagram of the electrical system to generate pulsed direct current is shown in Supplementary Fig. 2. A capacitor bank that can reach voltage up to 500 V with a total capacitance of 0.624 F was used. The capacitor is charged by a DC supply. A variable-frequency drive (VFD) was used to generate the pulse voltage with the frequency (f) ranging from 0 to 1000 Hz, while in this work, $f = 1000$ Hz was used. The duty cycle (or the ON state period) is tunable, and in this work, the duty cycle of 5% or 10% was used. The current profile was recorded using a Multifunction I/O (NI USB-6009) controlled by LabView. The carbon paper was used as the heater, which was secured on a graphite block and then connected to electrical system through two graphite electrodes that are inert to Cl₂. For the carbon paper with size of 1×3 cm², the resistance is ~ 0.7 Ω , which is appropriate for the Joule heating. We note that an appropriate resistance is critical for the effective heating (see Discussion in Supplementary Note 4).

Electrothermal chlorination and carbochlorination reactor and process.

In a typical small-scale experiment, the carbon paper size of 1×3 cm² was used for the sample mass of 100 mg. The sample was loaded on a carbon paper heater, which was connected to the

capacitor bank. The sample was put into a sealed quartz tube. After purging the system for 3×, Cl₂ was introduced at a flow rate of ~20 sccm for the small-scale sample, and ~40 sccm for the large-scale sample. The pulse current input brings the carbon paper heater to a desired temperature. The sample and gas temperatures instantly follow the pattern of heater temperature, as shown in Fig. 1g. The volatiles were deposited on the quartz tube. The chloride product is usually deliquescent, so the sample sealed in the quartz tube was transferred into a glove box, and the sample was then collected by scarping with a spatula from the quartz wall; the chlorides were loosely deposited on the inner quartz tube. The residue remaining on the carbon paper is also easily collected. In other cases, the sample was oxidized in air to isolate the pure metal oxide. The detailed experimental conditions for each experiment are shown in Supplementary Table 3. For Ta recovery from TCW, after the first-step ETC process, most of metal chlorides impurities were evaporatively removed from the residual Ta₂O₅ and SiO₂. Additionally, a water rinsing step can be used to further remove the metal chloride impurities.

Temperature measurement.

Temperatures below 200 °C were measured using an Infrared Thermometer (KIZEN LaserPro LP300). Temperatures between 200 and 1500 °C were measured using a thermometer (Micro-Epsilon, CTM-3SF75H2-C3). Temperatures between 1500 and 3000 °C were measured using a thermometer (Micro-Epsilon, CTRM-1H1SF100-C3). Both thermometers have a time resolution of 1 ms. Due to the available temperature range, different thermometers were used for the temperature measurement at voltage input of 30 – 60 V and 80 – 140 V, which leads to the discontinuity of the temperature – voltage curves (Fig. 1f).

Characterization.

Raman spectra were acquired using a Renishaw Raman microscope (laser wavelength of 532 nm, laser power of 5 mW, 50 × lens). SEM images were obtained using a FEI Quanta 400 ESEM FEG system at 20 kV. EDS spectra and maps were acquired using the same system equipped with an EDS detector. XPS were conducted using a PHI Quantera XPS system at a base pressure of 5 × 10⁻⁹ Torr. Elemental spectra were obtained with a step size of 0.1 eV with a pass energy of 26 eV. All the XPS spectra were calibrated using the standard C 1s peak at 284.8 eV. XRD was acquired using a Rigaku Smartlab II system configured with a Cu K α radiation ($\lambda = 1.5406 \text{ \AA}$). Since InCl₃

is very deliquescent, we used Kapton tape to seal the InCl_3 , avoiding contacting moisture during the XRD measurement. The broad peak at 26.3° in the XRD pattern (Fig. 2e) was ascribed to the tape substrate.

Sample digestion and ICP-MS measurement.

The samples were digested using acid and the metal contents were measured using ICP-MS. HNO_3 (67-70 wt%, TraceMetal™ Grade, Fisher Chemical), HCl (37 wt%, 99.99%, trace metal basis, MilliporeSigma), HF (48 wt%, 99.99%, trace metal grade for ICP analysis, MilliporeSigma), and ultrapure water (MilliporeSigma, ACS reagent for ultratrace analysis) were used for sample digestion. The ITO or the TCF waste samples were digested using an *aqua regia* method. Specifically, 50 mg of ITO or the TCE waste was dissolved using 3 mL of concentrated HCl and 1 mL of concentrated HNO_3 at 90°C for 2 h. Then, the solution was diluted to target concentrations using ultrapure water. In the recovery of In from ITO and the TCF wastes, the volatile was dissolved using 2 wt% HCl, while the residue was digested using the aforementioned *aqua regia* process. For the recovery of Ga from LED manufacturing wastes, the raw wastes and the residue after the ETC process were digested using aforementioned *aqua regia* process, and the volatile fraction was dissolved using 2 wt% HCl. For the recovery of Ta from TCW, all samples, including the TCW raw materials as well as the volatiles and the residues in both the first-step ETC and the second-step ETCC reactions, were digested using a HF:HCl: HNO_3 process. HF was required to dissolve the silicon in these samples⁴⁰. Specifically, 50 mg of the sample was dissolved in the mixed acid of 3 mL HCl, 1 mL HNO_3 , and 1 mL HF. Then, the solution was filtered using a sand core funnel (class F) and diluted to target concentrations using ultrapure water.

ICP-MS was conducted to measure the metal contents, using a Perkin Elmer Nexion 300 ICP-MS system. The below standards were used: Periodic Table mix 1 (MilliporeSigma, 33 elements of Al, As, Ba, Be, Bi, B, Ca, Cd, Cs, Cr, Co, Cu, Ga, In, Fe, Pb, Li, Mg, Mn, Ni, P, K, Rb, Se, Si, Ag, Na, Sr, S, Te, Tl, V, and Zn, 10 mg L^{-1} each, in 10 wt % HNO_3 containing HF traces), Periodic Table mix 2 (MilliporeSigma, 17 elements of Au, Ge, Hf, Ir, Mo, Nb, Pd, Pt, Re, Rh, Ru, Sb, Sn, Ta, Ti, W, and Zr, 10 mg L^{-1} each, in 5% HF and 1% HCl containing HNO_3 traces), individual standard of In, Sn, Y, Ta, Ni, Fe, Ta, Cu, and Mn (MilliporeSigma, 1000 mg L^{-1} in 2% HNO_3), and Si (Agilent Technologies, 1000 g L^{-1} in water with dilute HNO_3 and HF acid). For the total quantification of metal contents in wastes, including TCF and TCW, the mixture standards

were used. For the In recovery from ITO, In and Sn standards were used with Y as the inner standard. For the In recovery from TCF wastes, Cr, Au, In, Sn, and Mn standards were used with Y as the inner standard. For the Ga recovery from LED manufacturing wastes, Au, Ag, Ga, and Si standards were used with Y as the inner standard. For the Ta recovery from TCW, Ta, Si, Cu, Fe, Ni, and Mn standards were used with Y as the inner standard. All samples were measured triplicate to afford the standard deviations.

Technoeconomic analysis.

Four scenarios were considered in the TEA: (1) The ETC process, including the following processing blocks: N₂ introduction for purging and its recovery for reuse, Cl₂ introduction for chlorination, chlorination of mixed oxide feedstocks using an electrothermal reactor, off-gas (O₂ and unreacted Cl₂) separation using a distillation column and the recovery of Cl₂, calcination of chloride to convert it to oxide using a rotary kiln, and an acid plant to capture the HCl off-gas and production of the hydrochloric acid by-product; (2) the ETCC process, including the following processing blocks: N₂ introduction for purging and its recovery for reuse, Cl₂ introduction for chlorination, carbon introduction for reaction, carbon chlorination of mixed feedstocks using an electrothermal reactor, off-gas (CO and unreacted Cl₂) separation using a distillation column and the recovery of Cl₂, the combustion of CO off-gas using a combustor, rotary kiln for chloride calcination, and acid plant for HCl capture and hydrochloric acid production; (3) the acid leaching – solvent extraction process, including the following blocks: acid leaching of mixed metal feedstocks, solvent extraction for metal separation, stripping for metal recovery in aqueous phase, precipitation of metal, filtration, calcination to obtain the metal oxide, acid and extractant recovery, and wastewater and acid waste treatment; (4) the alkaline digestion – selective leaching process, including the following blocks: alkaline calcination of mixed oxide feedstocks, acid leaching of the calcined materials, filtration, secondary acid leaching of the residue, filtration to obtain the metal oxide product, gas recovery, and wastewater and acid waste treatment.

The global production rates of the critical metals considered in this work (In, Ga and Ta) are in the order of 1000 tonne per year. Hence, we here considered three feed capacities ranging from 1 to 100 metric tonnes per year. For the CAPEX estimation, we considered the inside battery limits (ISBL), while outside battery limits and engineering and construction costs were not. As a preliminary estimate or “Class 4” estimate, we used the accuracy of $\pm 30\%$ according to the

Association for the Advancement of Cost Estimating International (AACE International). The detailed description of equipment, materials flows, processing parameters, energy consumption, and materials and energy expense inventory are shown in Supplementary Note 5. The sensitivity analysis was conducted via Monte Carlo simulation. The code used for the Monte Carlo simulation was written by the authors and is provided with this paper. Total equipment pre-exponential, operating parameters, materials consumptions, materials costs, and process costs, all with a Class 4 error (+/-30%), were each randomly varied using continuous triangular distributions for the simulation.

Life-cycle assessment.

The environmental impact is evaluated via LCA (Supplementary Note 6). The same four scenarios (i.e., ETC process, ETCC process, acid leaching – solvent extraction, alkaline digestion – selective leaching) used in the TEA study were considered here (Supplementary Figs. 32-33). The functional unit of this study is the metal separation from 1 tonne of mixed metal oxide feedstock. The system boundary is defined to be the input of mixed metal oxide and the output of separated metal oxides. Life-cycle inventory (LCI) data (Supplementary Data 2.7) for inputs are from Argonne National Laboratory GREET Model⁴¹ and ecoinvent 3.8 global averages⁴²; if not available in these database, the LCI data were cited from representative literatures. The LCI entries were converted into environmental impacts using the ReCiPe 2016 methodology⁴³. Three environmental impacts were considered in this work, including global warming potential (GWP) in 100 year (GWP 100a), cumulative energy demand (CEM), and water resource depletion (WRD). Monte Carlo simulation was conducted for the sensitivity analysis. The code used for the Monte Carlo simulation was written by the authors and is provided with this paper. Briefly, 10⁵ iterations were conducted over the process parameters including materials consumptions and process energy consumption, which are varied using continuous triangular distributions. The upper and lower limits for the triangular distribution were taken as +30% and -30% of the base values.

Data availability

The data supporting the findings of the study are available within the paper and its Supplementary Information. Other relevant data are available from the corresponding authors. Source Data file for the Supplementary Data is provided with this paper.

Code availability.

Source code and its description file for TEA and LCA are provided with this paper.

Acknowledgements

We thank Dr. Helge Gonnermann of Rice University for allowing us to use the FEM simulation software, Dr. Bo Chen of Rice University for helpful input with the XPS results, and Dr. Christopher Pennington for developing ICP-OES and ICP-MS methods. We thank Dr. Zhonglei Li, Hailong Zhao, and Dr. Jinping Tian for helpful discussion on the LCA and TEA. The funding of the research was provided by the Defense Advanced Research Projects Agency (HR00112290122), the US Army Corps of Engineers, ERDC (W912HZ-21-2-0050), and the Rice Academy Fellowship (Y.C.).

Author Contributions

B.D. conceived the idea. B.D. conducted the thermodynamic analyses. B.D., S.X., and C.K. built the chlorination equipment. B.D. and S.X. conducted the experiment with the help of J.S., Y.C., K.J., L.Q., and S.C. L.E. built and maintained the electrical system. B.D. conducted the numeric simulation. B.D. conducted the techno-economic analysis and life-cycle assessment and analyzed the results. B.D., S.X., and J.M.T. wrote the manuscript. All aspects of the research were overseen by J.M.T. All authors have discussed the results and given approval to the final version of the manuscript.

Competing interests

An US provisional patent application has been filed on the electrothermal chlorination and carbochlorination process for selective metal recovery from electronic wastes (US Patent App. 63/415,384). The patent applicant is Rice University, and the inventors are J.M.T., B.D., and C.K. This application has not yet been licensed. The authors declare no other competing interests.

References

- 1 Reck, B. K. & Graedel, T. E. Challenges in metal recycling. *Science* **337**, 690-695 (2012).

- 2 Sovacool, B. K. *et al.* Sustainable minerals and metals for a low-carbon future. *Science* **367**, 30-33 (2020).
- 3 Watari, T., Nansai, K. & Nakajima, K. Review of critical metal dynamics to 2050 for 48 elements. *Resour. Conserv. Recycl.* **155**, 104669 (2020).
- 4 Frenzel, M., Mikolajczak, C., Reuter, M. A. & Gutzmer, J. Quantifying the relative availability of high-tech by-product metals – The cases of gallium, germanium and indium. *Resour. Policy* **52**, 327-335 (2017).
- 5 Frenzel, M., Ketris, M. P., Seifert, T. & Gutzmer, J. On the current and future availability of gallium. *Resour. Policy* **47**, 38-50 (2016).
- 6 R. Matsuoka, K. Mineta, T.H. Okabe, Recycling process for tantalum and some other metal scraps, Proc. TMS Fall Extr. Process. Conf., 2004 (2004), pp. 689-696.
- 7 Martelo, L. M., Sousa, P. M. S., Silva, M. A. D. & Soares, H. M. V. M. A critical updated review of all stages of the tantalum recycling chain from waste of tantalum capacitors. *Chem. Eng. J.* **472**, 144917 (2023).
- 8 U.S. Department of Energy's Strategy to Support Domestic Critical Mineral and Material Supply Chains (FY 2021–FY 2031).
- 9 Ghosh, B., Ghosh, M. K., Parhi, P., Mukherjee, P. S. & Mishra, B. K. Waste Printed Circuit Boards recycling: an extensive assessment of current status. *J. Clean. Prod.* **94**, 5-19 (2015).
- 10 Deng, B. *et al.* Urban mining by flash Joule heating. *Nat. Commun.* **12**, 5794 (2021).
- 11 Ogunseitan, O. A., Schoenung, J. M., Saphores, J.-D. M. & Shapiro, A. A. The Electronics Revolution: From E-Wonderland to E-Wasteland. *Science* **326**, 670-671 (2009).
- 12 Olivetti, E. A. & Cullen, J. M. Toward a sustainable materials system. *Science* **360**, 1396-1398 (2018).
- 13 Raabe, D., Tasan, C. C. & Olivetti, E. A. Strategies for improving the sustainability of structural metals. *Nature* **575**, 64-74 (2019).
- 14 Sun, Z. *et al.* Toward sustainability for recovery of critical metals from electronic waste: the hydrochemistry processes. *ACS Sustain. Chem. Eng.* **5**, 21-40 (2017).
- 15 Jadhav, U. & Hocheng, H. Hydrometallurgical recovery of metals from large printed circuit board pieces. *Sci. Rep.* **5**, 14574 (2015).
- 16 Lu, X. *et al.* A solid-state electrolysis process for upcycling aluminium scrap. *Nature* **606**, 511-515 (2022).

- 17 Stinn, C. & Allanore, A. Selective sulfidation of metal compounds. *Nature* **602**, 78-83 (2022).
- 18 Jena, P. K. & Brocchi, E. A. Metal extraction through chlorine metallurgy. *Miner. Process. Extr. Metall. Rev.* **16**, 211-237 (1997).
- 19 Xing, Z., Cheng, G., Yang, H., Xue, X. & Jiang, P. Mechanism and application of the ore with chlorination treatment: A review. *Miner. Eng.* **154**, 106404 (2020).
- 20 Niu, B., Chen, Z. & Xu, Z. Method for recycling tantalum from waste tantalum capacitors by chloride metallurgy. *ACS Sustain. Chem. Eng.* **5**, 1376-1381 (2017).
- 21 Niu, L.-p., Zhang, T.-a., Ni, P.-y., LÜ, G.-z. & Ouyang, K. Fluidized-bed chlorination thermodynamics and kinetics of Kenya natural rutile ore. *Trans. Nonferrous Met. Soc. China* **23**, 3448-3455 (2013).
- 22 Hans H. Glaeser, Mark J. Spoon, Fluidized bed process for chlorinating titanium-containing material and coke useful in such process, US5389353A
- 23 Terakado, O., Saeki, T., Irizato, R. & Hirasawa, M. Pyrometallurgical recovery of indium from dental metal recycling sludge by chlorination treatment with ammonium chloride. *Mater. Trans.* **51**, 1136-1140 (2010).
- 24 Gustafsson, A. M. K., Steenari, B.-M. & Ekberg, C. Recycling of CIGS solar cell waste materials: separation of copper, indium, and gallium by high-temperature chlorination reaction with ammonium chloride. *Sep. Sci. Technol.* **50**, 2415-2425 (2015).
- 25 Chen, Y. *et al.* Ultra-fast self-assembly and stabilization of reactive nanoparticles in reduced graphene oxide films. *Nat. Commun.* **7**, 12332 (2016).
- 26 Yao, Y. *et al.* Carbothermal shock synthesis of high-entropy-alloy nanoparticles. *Science* **359**, 1489-1494 (2018).
- 27 Luong, D. X. *et al.* Gram-scale bottom-up flash graphene synthesis. *Nature* **577**, 647-651 (2020).
- 28 Virolainen, S., Ibane, D. & Paatero, E. Recovery of indium from indium tin oxide by solvent extraction. *Hydrometallurgy* **107**, 56-61 (2011).
- 29 Angerer, T.; Luidold, S.; Antrekowitsch, H. Recycling potentials of the two refractory metals tantalum and niobium. Proceedings of EMC; GDMB: Clausthal-Zellerfeld, Germany, 2013; pp 1069–1084.

- 30 Niu, B., Chen, Z. & Xu, Z. Recovery of Tantalum from Waste Tantalum Capacitors by Supercritical Water Treatment. *ACS Sustain. Chem. Eng.* **5**, 4421-4428 (2017).
- 31 Chiera, N. M. *et al.* Formation and thermochemical properties of oxychlorides of niobium (Nb) and tantalum (Ta): Towards the gas-phase investigation of dubnium (Db) oxychloride. *Inorganica Chim. Acta* **486**, 361-366 (2019).
- 32 Sutter, R. C. Recovery of chlorine from air-chlorine mixtures. *J. Air Pollut. Control Assoc.* **7**, 30-31 (1957).
- 33 Otto Watzenberger, Joachim Pfeffinge, Selective separation and recovery of chlorine from gas mixtures, 1996, US5788743A.
- 34 Koleini, S. M. J., Mehrpouya, H., Saberyan, K. & Abdolahi, M. Extraction of indium from zinc plant residues. *Miner. Eng.* **23**, 51-53 (2010).
- 35 Xia, L., Wei, X., Wang, H., Ye, F. & Liu, Z. Valuable metal recovery from waste tantalum capacitors via cryogenic crushing-alkaline calcination-leaching process. *J. Mater. Res. Technol.* **16**, 1637-1646 (2022).
- 36 Yokoi, R., Watari, T. & Motoshita, M. Future greenhouse gas emissions from metal production: gaps and opportunities towards climate goals. *Energy Environ. Sci.* **15**, 146-157 (2022).
- 37 Deng, B. *et al.* Rare earth elements from waste. *Sci. Adv.* **8**, eabm3132 (2022).
- 38 Jovičević-Klug, M., Souza Filho, I. R., Springer, H., Adam, C. & Raabe, D. Green steel from red mud through climate-neutral hydrogen plasma reduction. *Nature* **625**, 703-709 (2024).
- 39 Stewart, E. S. & Lemieux, P. M. in *IEEE International Symposium on Electronics and the Environment, 2003.* 271-275.
- 40 Xu, J., Guo, Y., Yang, S., Hohl, S. V. & Zhang, W. Reliable determination of SiO₂ concentrations in sediments via sequential leaching and ICP-OES/MS analysis. *J. Geochem. Explor.* **242**, 107090 (2022).
- 41 Argonne GREET Model, <https://greet.anl.gov/databases>.
- 42 Ecoinvent-Association ecoinvent 3.8, <https://ecoinvent.org/the-ecoinvent-database/>.
- 43 Huijbregts, M. A. J. *et al.* ReCiPe2016: a harmonised life cycle impact assessment method at midpoint and endpoint level. *Int. J. Life Cycle Ass.* **22**, 138-147 (2017).